Frequency Response of Blower/Duct/Plenum Fluid Systems

F. R. Goldschmied*
Westinghouse Electric Corporation, Pittsburgh, Pa.

and

D. N. Wormley†
Massachusetts Institute of Technology, Cambridge, Mass.

An analytical and experimental study has been made of the aerodynamic frequency response of the basic blower/duct/plenum system, which is one of the elements of the lifting air cushion system of surface-effect ships. An analysis has been developed that includes unstalled blower dynamics, distributed-duct effects, and plenum flexible-wall effects. Theoretical predictions may be made of pressure amplitude ratios at several system locations for variable-frequency sinusoidal modulation of the plenum exit area, of the duct discharge area, or of the blower's inlet guide-vanes. Experimental frequency-response data have been obtained in a 40 HP blower/duct/plenum laboratory system for three blower speeds, over a range of frequencies up to 50 Hz, using rotating butterfly valves at the plenum exit or at the duct discharge. These data have compared well with the analytical predictions up to ~25 Hz and thus the theoretical method may be considered as validated for the lower frequencies.

Nomenclature

A_d = duct area, ft^2
A_e = exit area, ft^2
A_p = plenum effective wall area, ft^2
A_1 (A_2) = amplitudes of area variation defined in Eqs. (21) and (22), ft^2
c_0 = velocity of sound in air (fps)
C = plenum capacitance, ft^5/lb)
d = fan impeller diameter, ft
f_d = duct resonant frequency, Hz
f_p = frequency of peak response Hz
I = duct fluid inertance, lb-sec^2/ft^5
j = $\sqrt{-1}$
k = polytropic constant for air, 1.4 for an adiabatic process
K_p = effective plenum wall stiffness, lb/ft
L_d = duct length, ft
n = fan speed, rps
N = number of blades in fan
P = pressure, psf
P_a = atmospheric pressure, psf
P_d = pressure in duct, psf
P_f = fan outlet pressure, psf
P_p = plenum pressure, psf
Q = volume flow, ft^3/sec
Q_d = flow in duct, ft^3/sec
Q_e = flow exiting from plenum, ft^3/sec
Q_f = fan flow, ft^3/sec
Q_0 = nominal flow through system, ft^3/sec
R_d = duct resistance, lb-sec/ft^5
R_e = exit resistance, lb-sec/ft^5
R_f = fan resistance, lb-sec/ft^5
S = La Place transform variable, 1/sec
t = time, sec
T_e = duct delay time, sec
u = fan impeller tip speed, fps
V = plenum volume, ft^3
x = positive along duct, ft
y = plenum wall position, ft
Z_c = duct surge impedance, lb-sec/ft^5
α_d = duct valve modulation gain, fps
α_e = exit valve modulation gain, fps
Δ ( ) = increment of quantity ( ) above reference value
λ = fan blade angle, rad
ω = angular frequency, rad/sec
ϕ = fan flow coefficient
ψ = fan pressure coefficient
ρ = fluid density, slug/ft^3
τ = a system time constant, sec
τ_c = fan time constant, sec
τ_p = plenum time constant, sec
( )$_0$ = nominal value of quantity ( )

Received March 19, 1976; revision received Aug. 4, 1976. This work has been funded by Textron's Bell Aerospace Co. and by Westinghouse Electric Corp.

Index categories: Nonsteady Aerodynamics; Marine Vessel Systems, Surface.

*Advisory Scientist, Research Laboratories. Associate Fellow, AIAA.

†Associate Professor, Department of Mechanical Engineering.

I. Introduction

SURFACE effect ships and air cushion vehicles may show dynamic motion problems of sufficient severity to affect crew comfort and effectiveness on long missions, unless secondary suspensions are provided. On the other hand, even when ship motion is not a problem, pressure pulsations may occur in the air cushion and seal system, as shown both by numerical simulation and by actual experimental data, which can have a major impact on structural and machinery design. The air cushion lifting system is one of extreme dynamic complexity because of the following features: 1) multiple blower/duct units discharging in parallel into the plenum; 2) blower rpm variation; 3) exit air resistance dictated by ship motion, sea waves, and flexible seal skirt deformation; 4) air cushion plenum capacitance dictated by ship motion, sea waves, seal skirt deformation, and structural plenum elasticity; 5) two-dimensional acoustic effect in plenum; 6) spatial, as well as temporal, pressure variations in plenum, dictated by combination of previous effects.

A review of the technical literature discloses that numerical simulation studies of surface effect ships assume quasisteady blower operation, at best using the actual blower pressure/flow curve (up to stall) and at worst using a

linearized performance about a given operating point. The latest summary of the SES dynamic stability analysis is well-presented by Shih, et al.[1] The simulation of the actual motion of a specific air cushion vehicle (Jeff-B) is given in an excellent study by Cummings, et al.[2] The blower rpm dynamics have been investigated by Schneider and Kaplan.[3] Very extensive numerical simulation studies of the 100-B SES are presented by Grant,[4] Myers,[5] and Cagle.[6] Other numerical studies of the XR-3 test craft are presented by Forbes[7] and Finley.[8] An earlier motion analysis and fan system design method is given by Rajan and Csaky.[9]

Thus the present investigation has been motivated to fulfill a need for understanding the dynamics of the basic blower/duct/plenum fluid system, with a single blower in the unstalled regime, at constant rpm. Even the frequency response of the classic case of viscous compressible fluids in rigid tubes with closed chamber termination[10] can show a complete range of resonant pressure amplitudes and frequencies as a function primarily of the Stokes Number and of the chamber/duct volume ratio. The blower/duct/plenum dynamic interaction problem is more difficult by several orders of magnitude.

II. System Description and Instrumentation

The basic experimental system considered in this study is illustrated in Fig. 1. The system comprises a Westinghouse 4027-B DWDI centrifugal blower with a 27-in. diam. impeller, a 16-ft long duct with 28.75-in. × 38.75-in. cross-sectional dimensions (7.5 ft^2 area), and a 200-ft^3 plenum chamber with 60-in. × 60-in. × 96-in. dimensions. The flow exits from the plenum through two 12-in. diam. ASME aluminum nozzles, which provide the proper system resistance for the blower to run at approximately its maximum-efficiency point.

The steady-state experimental performance of the blower is presented in Fig. 2 in terms of static-pressure coefficient ψ_s and static-efficiency η_s against the flow coefficient ϕ. The test data were taken at four speed values, i.e., 1000, 1250, 1550, and 1750 rpm, and appear to collapse on a single plot in the dimensionless representation, thus demonstrating exact aerodynamic similarity.

The flow coefficient ϕ is defined as follows

$$\phi = \frac{Q}{\frac{\pi}{4} d^2 u}$$

where Q is the blower flow rate in ft^3/sec, d is the impeller tip diameter in ft, and u is the impeller tip speed in fps. The pressure coefficient ψ is defined as follows

$$\psi = \frac{\Delta P}{\frac{1}{2} \rho u^2}$$

where ΔP is the pressure rise, static or total, in lb/ft^2 and ρ is the fluid mass density in lb-sec^2/ft^4.

At the maximum efficiency point at 1750 rpm, the blower delivered a flow of the order of 20,000 cfm against 40 psf static-pressure. This blower was a standard Westinghouse industrial unit with ample radial clearance between rotating impeller and fixed inlet (0.075 in. average), equipped with inlet guide vanes for negative-flow control; it was chosen because it is representative of the aerodynamic design class that would be used for surface-effect ship cushion applications.

To eliminate sheet-metal flutter, the duct and the plenum were fabricated with ¾-in.-thick plywood reinforced with heavy steel angles and braces. Steady-state static pressures were obtained in the duct wall at 1 ft from the blower's flange and at 1 ft from the duct's termination into the plenum; the first station has been termed "blower" and the second "duct." A third static-pressure location was placed in the plenum at 1 ft from the top; this station has been termed "top plenum." Four taps were used at each station to average the pressure measured by a 48-in. Meriam inclined water manometer.

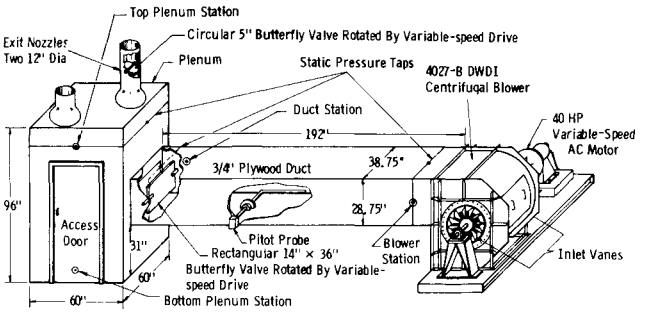

Fig. 1 Schematic diagram of experimental blower-duct-plenum system.

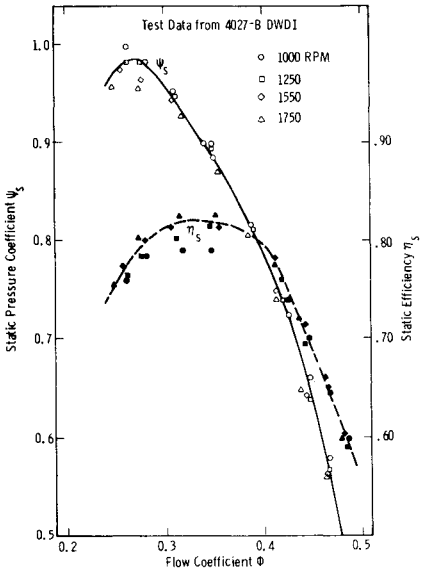

Fig. 2 Static blower performance.

At each station, a single Setra Model 237 1.0 psid transducer was also installed to record the time-dependent static wall pressure. In this manner, the Setra electrical output signal could always be compared to the Meriam manometer reading at the given station. A fourth Setra transducer was located in the plenum 1 ft from the bottom; this station was termed "bottom plenum."

Before beginning the experimental frequency response program with forced system excitation (rotating butterfly valves), it was deemed advisable to observe the flow dynamics of the test system without any forced excitation. A total-pressure probe with a Setra transducer was placed at the midpoint of the duct centerline and the blower was run approximately at its maximum efficiency point, eliminating stall effects and consequent surging.

The results are given in Table 1 for the amplitude ratio, at seven speeds and five inlet guide-vanes settings: The overall average ratio is 0.127; i.e., the peak-to-peak average total-pressure pulsation is nearly 13% of the mean total-pressure blower output for the centrifugal blower running near maximum efficiency in the given blower/duct/plenum test system without any forced external excitation of any kind.

The other important result is the major frequency of these total-pressure pulsations; these data are shown in Table 2, again for seven speeds and five inlet guide-vane settings: The average major frequency is three-quarters of the rpm value. The frequency data points are plotted in Fig. 3 and clearly outline the linear dependence on rpm, regardless of inlet guide-vane angle setting.

The fact that this self-excitated pulsation occurred at design flows and for all inlet guide-vane settings rules out the classical rotating stall as the source. Instead, the source is due to the dynamic flow instability between the two inlets of the DWDI blower; this phenomenon has already been reported by Cheshire[11] and by Dussourd and Putnam[12] for double-inlet centrifugal compressors. It should be reported that the frequency (75% rpm) is higher than that reported for rotating stall. Lennemann and Howard[13] have conducted a visual study of rotating stall in shrouded backward-curved centrifugal impellers and have reported frequencies from 50 to 66% rpm.

Gilkey, Rogers, Wyrough, Pettersson and Howitt[14] have considered pressure surging of centrifugal blowers in a number of central-station power plants and have reported that the only common relationship known between the several units was that the pulsating frequency corresponded to 66% rpm in all cases.

III. Frequency Response Measurements

In measuring the dynamic characteristics of the experimental blower/duct/plenum system, the first step consisted in establishing the steady-state operation approximately at the maximum-efficiency point of the blower, well away from the stall point. The present study is concerned with unstalled impeller flow only and thus care was taken to avoid stall in the entire test range. The blower was operated at three speeds; i.e., 1000 rpm, 1350 rpm, and 1750 rpm; the plenum exit butterfly was operated from 0 to 50 Hz while the duct damper butterfly was operated from 0 to 25 Hz. The blower pressure ranged from 14-45 psf and the flow delivery ranged 150-265 cfs. In reference to the dimensionless performance plot of Fig. 2, the blower was operated approximately at $\phi = 0.32$ and $\psi = 0.90$.

After the given steady-state operating point was achieved, dynamic disturbances to the system could be introduced in two basic ways:

1) Through a rotating butterfly valve installed in one of the two plenum exit nozzles. This valve consisted of a 5-in.-diam. circular disk mounted on a rotatable shaft in the center of the 12-in. diam. nozzle and covering only 9% of the total plenum discharge area in its "closed" position.‡ The steady-state pressure differentials ΔP_0 seen in the plenum between the "open" and "closed" valve position were ~0.78 psf at 1000 rpm, ~1.30 psf at 1350 rpm, and ~2.60 psf at 1750 rpm. The butterfly valve was then made to rotate at increasing speeds so as to cover the desired frequency range.

2) Through a rotating butterfly damper installed at the end of the duct (inlet to the plenum). The damper consisted of a flat 14-×36-in. rectangular plate mounted on a rotatable shaft in the center of the duct and covering 47% of the duct cross-sectional area. The steady-state pressure differential ΔP_0 seen in the plenum between the "open" and "closed" damper positions were ~1.55 psf at 1000 rpm, ~3.10 psf at 1350 rpm, and ~4.65 psf at 1750 rpm. The butterfly damper was then made to rotate at increasing speed so as to cover the desired frequency range.

The experimental procedure was designed to produce the ratio of the dynamic peak-to-peak pressure amplitude (as seen on the oscilloscope from the Setra transducer) ΔP_{p-p} over the steady-state pressure differential ΔP_0 (as seen both by the Meriam manometer and by the Setra transducers) created by the butterfly in fixed "open" and fixed "closed" positions. This pressure amplitude ratio was then to be shown as a function of frequency in the classical manner of the BODE plot (frequency response).

‡It is to be noted that in other investigations, such as that reported by Durkin and Langhi,[15] the butterfly covered ~100% of the total plenum discharge area and forced the blower into stall.

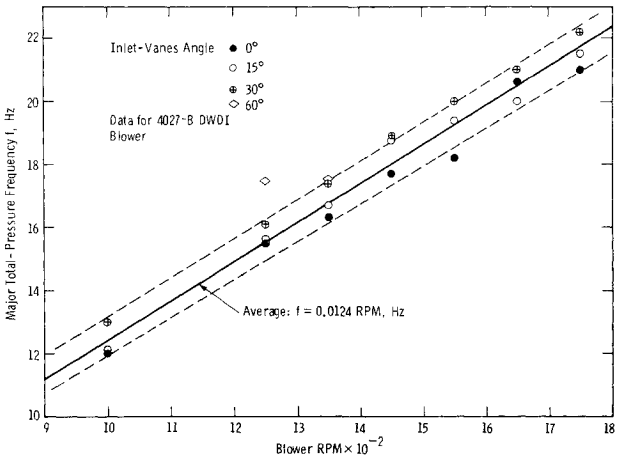

Fig. 3 Frequency of major total-pressure fluctuations without system excitation.

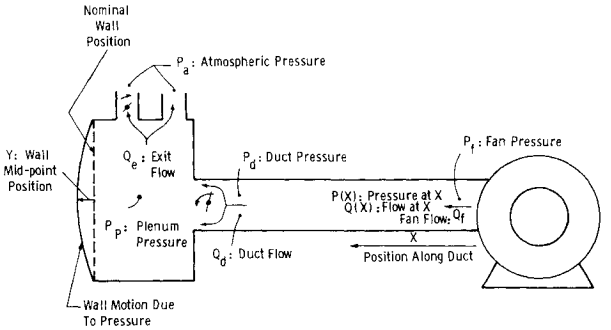

Fig. 4 Definition of nomenclature.

IV. General System Analysis

An analytical model has been developed, along the lines of Ref. 16, to describe the dynamic performance of blower/duct/plenum systems. The analysis is developed specifically to predict the pressure response at three system locations (plenum, duct's, and blower's discharge, see Fig. 1) to resistance variations caused by the rotation of a small round butterfly valve at the plenum's exit or of a rectangular damper at the duct's exit into the plenum. Since these devices create a quasisinusoidal disturbance with a frequency determined by the known rpm, the frequency-response approach has been followed for the theoretical development.

In the sections below, the basic equations describing each part of the system are presented and summarized. These equations are linearized and then combined to form a complete dynamic model of the blower/duct/plenum system. The nomenclature used in the analysis is defined in Fig. 4.

A. The Plenum Chamber

The plenum chamber has been modeled by assuming that spatial variations within the chamber may be neglected in regard to fluid density and pressure. For actual SES plenums, with typical large dimensions in length and width, two-dimensional acoustic wave effects will require detailed consideration and the location of the blower's discharge duct within the plenum will be of dynamic significance. It has not been possible to enter into the above complexities within the limited scope of the present study.

Mass conservation for the plenum chamber, neglecting spatial variations, may be written as

$$\rho Q_d - \rho Q_e = \frac{\mathrm{d}}{\mathrm{d}t}(\rho V) = V\frac{\mathrm{d}\rho}{\mathrm{d}t} + \rho\frac{\mathrm{d}V}{\mathrm{d}t} \qquad (1)$$

where ρ is the fluid mass density, Q_e the volumetric flow rate exiting from plenum, Q_d the volumetric flow rate entering into plenum from duct, V the plenum volume, t the time.

When the equation of state for air is employed in a linear form

$$\frac{\Delta\rho}{\rho} = \frac{\Delta P_p}{kP_p} \tag{2}$$

where k is the polytropic constant, P_p the plenum pressure, $\Delta(\ )$ the increment of quantity $(\ )$ from steady-state value, and when the change in volume of the plenum chamber due to flexible walls§ is represented as

$$V = V_0 + \Delta V = V_0 + A_p y \tag{3}$$

where V_0 is the nominal plenum chamber volume, A_p the effective wall area of expansion, y the wall geometrical midpoint displacement, $\Delta V = A_p y$ the incremental plenum volume, and the expansion of the chamber is given by balancing the pressure force on the flexible wall against the effective wall stiffness multiplied by the midpoint displacement

$$(P_p - P_a)A_p = K_p y \tag{4}$$

where K_p is the effective plenum chamber wall stiffness at midpoint, based upon effective wall area A_p.

Now combining Eqs. (1)-(4) yields a linear equation for the plenum chamber

$$C\frac{d\Delta P_p}{dt} = \Delta Q_d - \Delta Q_e \tag{5}$$

where C is the effective plenum capacitance. The effective plenum capacitance now includes a term due to the fluid compressibility (involving the nominal plenum volume V_0) and a term due to the wall stiffness (involving K_p)

$$C = \frac{V_0}{kP_{c0}} + \frac{A_p{}^2}{K_p} \tag{6}$$

where P_{co} is the nominal absolute plenum pressure.

If the chamber walls are rigid, then $K_p \to \infty$ and the capacitance reduces to that of a rigid plenum, i.e.

$$C = \frac{V_0}{kP_{c0}}$$

It is expected that the large flat light-weight structure of the SES plenum will exhibit considerable structural flexibility and that, therefore, the variable capacitance will be a very important factor in the SES fluid systems analysis.

The flows into the plenum and out of the plenum may be related directly to the pressure drops across the plenum exit area (ASME nozzles) and across the plenum inlet area (duct cross-sectional area). Both the exit area and the inlet area may be varied dynamically by rotating butterfly valves, thus the incremental flow through each area is due to a pressure increment and/or an area increment.

The linearized incremental flows may be expressed as

$$\Delta Q_e = \frac{\Delta P_p}{R_e} + \alpha_e \Delta A_e \tag{7}$$

$$\Delta Q_d = \frac{\Delta(P_d - P_p)}{R_d} + \alpha_d \Delta A_d \tag{8}$$

§The plenum was fabricated with 3/4-in.-plywood walls; in-and-out motion of the vertical flat panels could be observed visually.

where R_e is the exit resistance, R_d the inlet resistance from duct, α_e the exit area modulation gain, α_d the duct area modulation gain, ΔA_e the incremental change in exit area, ΔA_d the incremental change in duct area.

The values of resistance and of area modulation gains may be related directly to the flow and areas at the nominal system operating point if it is assumed that both orifices are described by the standard quadratic equation. In this case the linear resistance and area gain factors are

$$R_e = \frac{2(P_p - P_a)_0}{Q_0} \tag{9}$$

$$R_d = \frac{2(P_d - P_p)_0}{Q_0} \tag{10}$$

$$\alpha_e = \frac{Q_0}{A_{e0}} \tag{11}$$

$$\alpha_d = \frac{Q_0}{A_{d0}} \tag{12}$$

where $(\ )_0$ indicates the nominal operating point value, Q_0 the nominal flow through system.

When Eqs. (1)-(12) are combined, the basic plenum equation may be written in Laplace transform notation which is convenient for frequency response analysis as

$$\tau_p S\Delta P_p + \Delta P_p = \frac{R_e R_d}{R_e + R_d}\left[\frac{\Delta P_d}{R_d} + \alpha_d \Delta A_d - \alpha_e \Delta A_e\right] \tag{13}$$

where

$$\tau_p = C\frac{R_e R_d}{R_e + R_d}$$

and S is the Laplace transform variable. The quantity τ_p is the basic plenum chamber time constant, which is a function of the plenum capacitance and of the inlet (duct) and exit resistances.

The parameter values used for the analysis of the experimental system described above are listed in Table 3 for the flexible-wall plenum, for 1000 rpm, 1350 rpm, and 1750 rpm blower speeds.

B. The Duct

The duct in the experimental system is long enough (16 ft) so that in the frequency range of interest (0-50 Hz) wave transmission effects are important. Since the duct length to cross-section dimension is large (16/3), the duct has been modeled as a one-dimensional acoustic-wave transmission system. In addition, since frictional resistance in the duct is small as compared with other resistances in the system, the duct is modeled as lossless. In practice, the duct resistance may be lumped into the resistances at each end of the duct.

Thus, the one-dimensional acoustic-wave equations describing the pressure and flow at any location in the duct are as follows

$$\frac{\partial^2 Q}{\partial x^2} = \frac{1}{c_0{}^2}\frac{\partial^2 Q}{\partial t^2} \tag{14}$$

$$\frac{\partial^2 P}{\partial x^2} = \frac{1}{c_0{}^2}\frac{\partial^2 P}{\partial t^2} \tag{15}$$

where x is the axial position along duct, t the time, Q the flow in the duct at position x and time t, P the pressure in the duct at position x and time t, and c_0 the velocity of sound in the duct. These equations are linear, homogeneous, partial differential equations classically known as the Wave Equations.

Table 1 Peak-to peak total-pressure amplitude ratio

	Inlet Guide-Vanes Setting				
RPM	0°	15°	30°	45°	60°
1750	0.125	0.100	0.100	0.090	0.130
1650	0.120	0.120	0.120	0.120	0.130
1550	0.100	0.110	0.120	0.100	0.130
1450	0.120	0.120	0.140	0.100	0.120
1350	0.140	0.140	0.140	0.120	0.130
1250	0.140	0.180	0.160	0.110	0.140
1000	0.180	0.140	0.180	0.120	N.A.
Average:	0.132	0.130	0.137	0.109	0.130

Table 2 Major frequency of total-pressure fluctuations

	Inlet Guide-Vanes Setting					
RPM	0°	15°	30°	45°	60°	Average
1750	21.0 Hz	21.5 Hz	22.2 Hz	--	--	21.56 Hz
1650	20.6	20.0	21.0	--	--	20.53
1550	18.2	19.4	20.0	--	--	19.20
1450	17.7	18.9	18.9	--	--	18.50
1350	16.3	16.7	17.4	--	17.5 Hz	16.97
1250	15.5	15.6	16.1	--	17.5	16.17
1000	12.0	12.1	13.0	--	--	12.36

Table 3 Plenum chamber parameters with flexible walls

		BLOWER SPEED		
PARAMETER		1000 RPM	1350 RPM	1750 RPM
PLENUM VOLUME	V_o ft^3	200.0000	200.0000	200.0000
PLENUM CAPACITANCE	C ft^5/lb	0.1518	0.1518	0.1518
PLENUM PRESSURE	P_p lb/ft^2	12.4292	22.6522	38.0644
PLENUM TIME CONSTANT	τ_p sec	0.0038	0.0051	0.0066
EXIT AREA	A_e ft^2	1.5069	1.5069	1.5069
EXIT RESISTANCE	R_e lb sec/ft^5	0.1658	0.2239	0.2902
EXIT FLOW GAIN	α_e ft/sec	99.4779	134.2951	174.0864
DUCT RESISTANCE	R_d lb sec/ft^5	0.0293	0.0395	0.0512
DUCT FLOW GAIN	α_d ft/sec	43.9885	59.3845	76.9799

Table 4 Duct parameters

		BLOWER SPEED		
PARAMETER		1000 RPM	1350 RPM	1750 RPM
DUCT EFFECTIVE LENGTH	L_d ft	20.25	20.25	20.25
DUCT AREA	A_d ft^2	7.7100	7.7100	7.7100
SURGE IMPEDANCE	Z_c lb sec/ft^5	0.3300	0.3300	0.3300
DUCT DELAY TIME	T_c sec	0.0181	0.0181	0.0181
PRESSURE INPUT TO DUCT	P_f lb/ft^2	14.226	26.6497	44.7816
FLOW INPUT TO DUCT	Q_f ft^3/sec	149.9011	202.3665	262.3269
DAMPER RESISTANCE	R_d lb sec/ft^5	0.0293	0.0395	0.0512
DAMPER FLOW GAIN	α_d ft/sec	43.9885	59.3845	76.9799

The equations may be partially solved and written in operational Laplace transform notation and expressed as pressures and flows at each end of the duct as shown by Sweet, et al.[6]

$$\Delta P_d = [\cosh T_e s]\Delta P_f - [Z_c \sinh T_e s]\Delta Q_f \tag{16}$$

$$\Delta Q_d = [\frac{-\sinh T_e s}{Z_c}]\Delta P_f + [\cosh T_e s]\Delta Q_f \tag{17}$$

where P_f is the blower pressure at duct's end, Q_f the blower flow into duct, T_e the duct's delay time, and Z_c the duct's surge impedance.

The duct's delay time is simply

$$T_e = \frac{L_d}{c_0} \tag{18}$$

and the duct surge impedance is

$$Z_c = \rho \frac{c_0}{A_d} \tag{19}$$

where L_d is the effective duct length, A_d the duct area, and c_0 the velocity of sound in duct.

Equations (16) and (17) are in a form that can be combined directly with the plenum equations to describe the mathematical model of the plenum/duct system. It is to be noted that the effective length of the duct comprises the actual length of 16 ft plus the length of the blower housing discharge of 1 ft plus one-half of the blower's impeller peripheral length of 3.25 ft.

The parameter values used for the analysis of the experimental system described above are listed in Table 4 for 1000 rpm, 1350 rpm, and 1750 rpm blower speeds.

C. The Blower

A linearized model for the blower has been developed on the basis of the actual 4027-B steady-state performance, as shown in Fig. 2 ($\phi = 0.32$ and $\Psi = 0.93$) and on the basis of the frequency response theory of Ohashi.[17] Ohashi formulated a linearized dynamic model for turbopumps with unseparated flow that relates dynamic variations in pressure rise across the blower to the corresponding instantaneous flow through the blower. The double-inlet instability has not yet been incorporated in the blower model, since it is really a problem of multiple parallel blower operation.

Generally the response of the blower is assumed to be quasi-steady regardless of the frequency involved. This means that, at any time, for any instantaneous flow rate, the pressure generated by the blower corresponds to the steady-state pressure/flow curve and also that the pressure/flow phase angle remains unchanged at 180°. Actually, like any other machine or device, the centrifugal blower will have some definite frequency response function or Bode plot. Such frequency response has never been taken experimentally by Westinghouse or any other U.S. blower manufacturer, as far as it is known to the authors after an exhaustive literature search.

In his experimental work at NASA Marshall Space Flight Center Ohashi used a centrifugal pump, Type 1 1/2 CCL/Buffalo Pumps, 6.32-in. impeller diameter, running at 3500 rpm to deliver 120 gpm at 150-ft head rise. The design flow coefficient was $\phi \cong 0.017$ and the design pressure coefficient was $\Psi \cong 0.8$. In the test program, the rpm was taken at 3600, 1800, and 900, the oscillating flow amplitude was limited to 10% of the mean flow and its frequency range was from 1 to 100 Hz; the mean flow was taken at the design point (ϕ_D) and at half-capacity ($1/2\,\phi_D$).

The dynamic results are presented in the conventional manner as the pressure-amplitude ratio and the phase shift against a frequency parameter; that is , what is generally termed the "frequency response" or BODE plot. Figure 5 shows the ratio of the actual pressure-rise ΔP to ΔP_{qs}, which corresponds to the steady-state performance for the measured instantaneous flow rate, plotted against a dimensionless frequency parameter ω_R. This parameter, which governs the similarity scaling for different sizes, rpm, and flows, is defined as follows

$$\omega_R = \frac{\cos\lambda_R}{B \cdot \phi^*} \frac{f}{n} \tag{20}$$

where

λ_R = equivalent stagger angle of impeller cascade
B = the number of impeller blades

ϕ^* = flow parameter: $\dfrac{Q}{\pi d_2 b_2 u} = \phi \dfrac{d_2}{4b_2}$

d_2 = impeller tip diameter, ft
b_2 = impeller tip width ft
u = impeller tip speed, ft/min

ϕ = flow coefficient: $\dfrac{Q}{(\pi/4) d_2{}^2 u}$
Q = flow rate, ft^3/min
f = imposed forced frequency, Hz
n = shaft speed, rps

Figure 5 shows also the corresponding phase shift between ΔP and ΔP_{qs} plotted against the frequency parameter ω_R. The Ohashi theory is also represented in Fig. 5.

It is of the greatest interest at this point to consider the experimental results of the 4027-B DWDI blower in the framework of Fig. 5. The computation of ω_R for the 4027 blower is as follows

$\cos\lambda_R$ $= \cos 55° = 0.573$

$\dfrac{b_2}{d_2}$ $= 0.4968$ = tip width ratio for double impeller

ϕ^* $= 0.176$ @ at maximum efficiency flow $\phi =$ 0.35 (total flow of double impeller)

$\dfrac{f}{n}$ $= 0.744$ = major frequency of Sec. III

Thus $\omega_R \simeq 0.242$ for all the frequencies plotted in Fig. 3. This value of ω_R is at the quasisteady limit according to the Ohashi theory

$$(\frac{\Delta P}{\Delta P_{qs}} > 0.90)$$

Thus it may be said that the blower will be quasisteady for frequencies below the line in Fig. 3 and that it will respond dynamically for frequencies above that line.

The Ohashi model may be summarized by the following equation written in Laplace transform notation

$$\left[\sqrt{\tau_c S + 1}\right]\Delta P_f = -R_c \Delta Q_f \tag{21}$$

where

τ_c = blower time constant

R_c = blower "resistance" $= -\dfrac{dP_f}{dQ_f}$
P_f = blower pressure
Q_f = blower flow

In Eq. (21), the blower time constant is a function of the dimensionless frequency ω_R of Eq. (20). For the purposes of Eq. (21) the blower time constant may be approximated as follows, from the impeller design and the rpm

$$\tau_c \approx \frac{\cos\lambda_R}{2B\phi^* n} \tag{22}$$

or

$$\omega_R = 2\tau_c \cdot f$$

If $\omega_R \cong 0.25$ is accepted as the dividing line between quasi-steady and dynamic blower operation, then the corresponding "critical" frequency is given by

$$f_0 \cong \frac{0.25}{2\tau_c} \tag{23}$$

The parameter values used for the analysis of the experimental system previously described are listed below in Table 5 for 1000 rpm, 1350 rpm, and 1750 rpm blower speeds.

D. System Model Summary

The equations derived for the blower/duct/plenum system may be combined and summarized as shown in Table 6, where the blower pressure ΔP_f, the duct pressure ΔP_d, and the plenum pressure ΔP_p are related directly to the variations in the plenum exit area ΔA_e and in the duct damper area ΔA_d.

When the area variations are considered to be sinusoidal, such as produced by the rotating butterfly valves, then

$$\Delta A_d = A_1 \sin(\omega t) \tag{24}$$

$$\Delta A_e = A_2 \sin(\omega t) \tag{25}$$

where A_1 and A_2 are amplitude or area variation. As previously shown, the plenum exit butterfly area was 9% of the total plenum exit area and the duct damper butterfly was 47% of the total duct area.

The equations summarized in Table 6 may be solved simultaneously to determine each pressure magnitude by replacing $S \rightarrow j\omega$ where $j = \sqrt{-1}$ and ω is the frequency and then by computing the resultant magnitude from the complex functions. A digital computer program has been used to carry out the computations over a frequency range 0-60 Hz for the case of the rigid plenum and for the case of the flexible-wall plenum. For convenient visual inspection, the flexible plenum results at 1750 rpm are plotted in Figs. 6, 7, and 8. Figure 6 presents the theoretical frequency response to plenum exit area modulation, Fig. 7 shows the response to duct damper area modulation, and Fig. 8 displays the response to inlet guide-vane modulation.

V. Experimental Verification of Analytical Predictions

The experimental frequency response data obtained in the present program are presented in Figs. 9-14, together with the

Table 5 Blower parameters

PARAMETER		BLOWER SPEED 1000 RPM	1350 RPM	1750 RPM
Impeller Diameter	D in.	27.0000	27.0000	27.0000
Flow Coefficient	ϕ (see Figure 4)	0.32	0.32	0.32
Pressure Coefficient	Ψ (see Figure 4)	0.93	0.93	0.93
Blower Flow	Q_f ft^3/sec	149.9011	202.3665	262.3269
Blower Pressure	P_f lb/ft^2	14.6226	26.6497	44.7816
Blower Resistance	R_c $lb\ sec/ft^5$	0.042	0.0566	0.0734
Blower Time Constant	τ_c sec	0.0100	0.0074	0.0057

Table 6 Summary of system equations

$$\begin{bmatrix} (\tau_p S + 1) & -\frac{R_e}{R_e + R_d} & 0 \\ -\frac{Z_c \sinh(T_e S)}{R_d} & \cosh(T_e S) + \frac{Z_c \sinh(T_e S)}{R_d} & -1.0 \\ 1.0 & -1.0 & -\frac{R_d}{R_f}\left[\cosh(T_e S) \cdot \sqrt{\tau_c S + 1}\right] - \left[\frac{R_d \sinh(T_e S)}{R_c}\right] \end{bmatrix} \cdot \begin{bmatrix} \Delta P_p \\ \Delta P_d \\ \Delta P_f \end{bmatrix} = \begin{bmatrix} \frac{R_e R_d}{R_e + R_d} \cdot \left[\alpha_d \Delta A_d - \alpha_e \Delta A_e\right] \\ -(Z_c \alpha_d \Delta A_d) \cdot \sinh(T_e S) \\ R_d \alpha_d \Delta A_d \end{bmatrix}$$

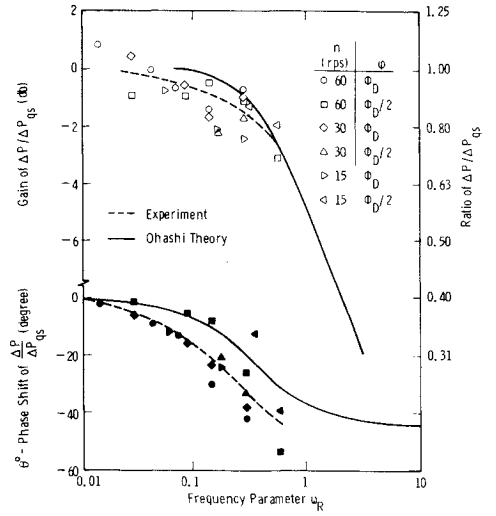

Fig. 5 Frequency response of Ohashi test pump: pressure amplitude ratio and phase angle (ref. 17).

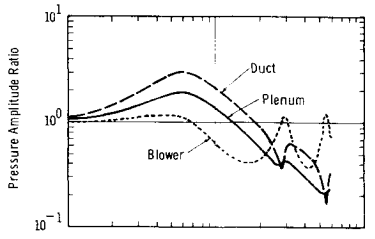

Fig. 6 Frequency response analysis with flexible plenum at 1750 rpm: pressure amplitude ratio for plenum exit area modulation.

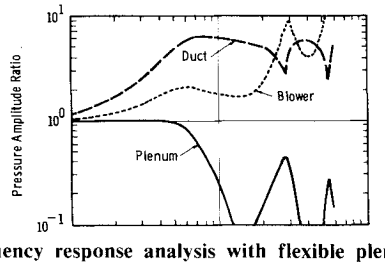

Fig. 7 Frequency response analysis with flexible plenum at 1750 rpm: pressure amplitude ratio for duct damper area modulation.

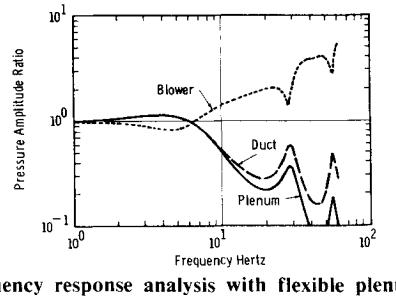

Fig. 8 Frequency response analysis with flexible plenum at 1750 rpm: pressure amplitude ratio for inlet guide-vane modulation.

predictions achieved with the rigid plenum theory and those obtained with the flexible plenum theory for 1750 rpm blower speed. The ratio of the peak-to-peak pressure differential is plotted on the vertical scale; the frequency of the area modulation caused by the rotating butterfly in Hz is plotted on the horizontal scale. Three blower speeds were employed, since speed is a significant fluid system parameter, i.e., 1000, 1350, and 1750 rpm. Also, three system locations were considered, since the results can be quite different at the several

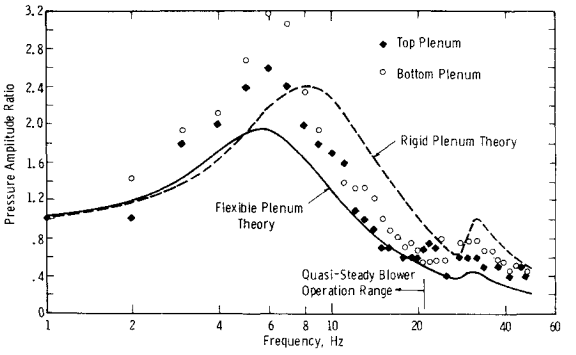

Fig. 9 Experimental frequency response at 1750 rpm to plenum exit area modulation: plenum location.

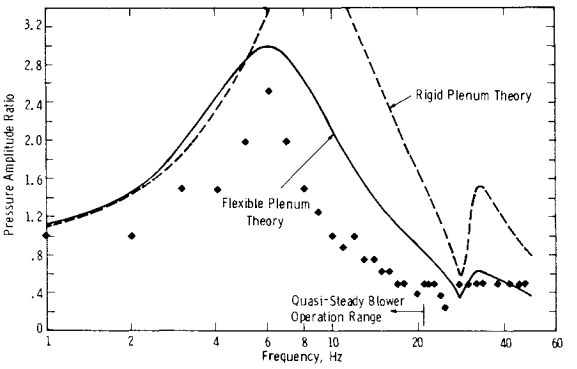

Fig. 10 Experimental frequency response at 1750 rpm to plenum exit area modulation: duct location.

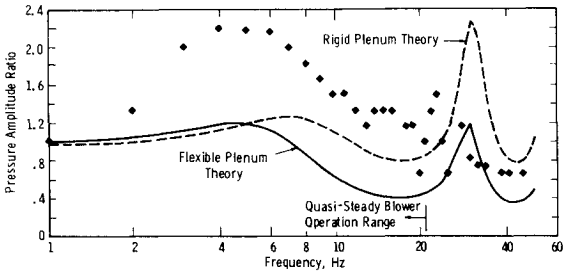

Fig. 11 Experimental frequency response at 1750 rpm to plenum exit area modulation: blower location.

locations: plenum, duct, and blower as indicated in Fig. 1. For the results at the plenum location, two sets of data points are shown: one set was taken 1 ft from the top of the plenum and the second set was taken 1 ft from the bottom of the plenum.

Also shown in each figure is the range of quasisteady blower operation below the frequency corresponding to $\omega_R = 0.24$; above this frequency, blower dynamic effects become increasingly significant. It is seen that resonant frequencies vary from 5 Hz to 30 Hz for this system, depending on the location observed, the blower rpm and the mode of system excitation; it is not possible to make simplified statements such as, "the resonant frequency of this system is XX Hz." In regard to the lift of the surface-effect ship, the plenum response is the one that counts; in regard to blower behavior such as stall, it is the blower response that must be considered.

Table 7 summarizes the first resonant (or antiresonant) frequencies and corresponding amplitude ratios for all the cases investigated both experimentally and theoretically. The frequency agreement is excellent; out of 18 cases, only three show a discrepancy larger than 2 Hz. The agreement is qualitatively good for the pressure amplitude ratio; this is all

Table 7 Summary of resonant frequencies and pressure amplitude ratios

System Excitation	Blower RPM	System Location	Frequency Hz		Pressure Amplitude Ratio	
			Theor.*	Exp.	Theor.	Exp.
Plenum Exit	1000	Plenum	6	5	2.66	2.50
Plenum Exit	1000	Duct	6	6	4.38	3.65
Plenum Exit	1000	Blower	28	26	3.18	1.15
Plenum Exit	1350	Plenum	6	6	2.30	2.60
Plenum Exit	1350	Duct	6	6	3.69	3.00
Plenum Exit	1350	Blower	30	30	1.91	1.65
Plenum Exit	1750	Plenum	6	6	1.93	2.60
Plenum Exit	1750	Duct	6	6	3.00	2.50
Plenum Exit	1750	Blower	5	5	1.18	2.20
Duct Damper	1000	Plenum	14	14	0.030	0.32
Duct Damper	1000	Duct	8	8	6.27	8.00
Duct Damper	1000	Blower	30	21	14.52	5.40
Duct Damper	1350	Plenum	14	13	0.045	0.30
Duct Damper	1350	Duct	8	7	6.27	8.00
Duct Damper	1350	Blower	30	22	11.58	5.00
Duct Damper	1750	Plenum	15	13	0.060	0.22
Duct Damper	1750	Duct	8	8	6.12	7.00
Duct Damper	1750	Blower	30	19	9.05	5.00

*Flexible Plenum Theory.

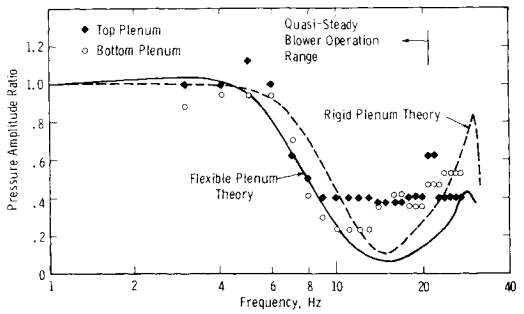

Fig. 12 Experimental frequency response at 1750 rpm to duct damper area modulation: plenum location.

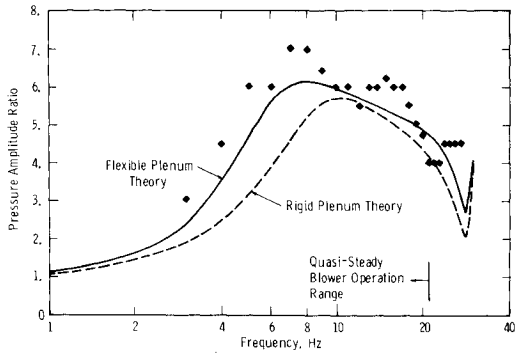

Fig. 13 Experimental frequency response at 1750 rpm to duct damper area modulation: duct location.

that can really be expected from a linearized inviscid theory. The highest resonant experimental amplitude ratio was 8 and the lowest experimental antiresonant amplitude ratio was 0.22. Thus it can be said that a broad range of amplitude ratios was studied in this program.

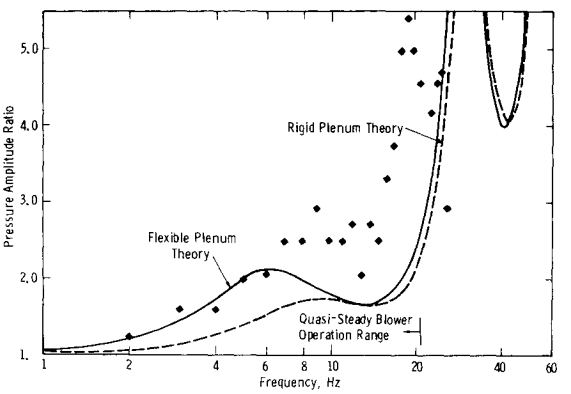

Fig. 14 Experimental frequency response at 1750 rpm to duct damper area modulation: blower location.

VI. Conclusions

Several important conclusions may be derived from all the above evidence.

1) The plenum can be rightfully assumed as one lumped capacitance because there is excellent agreement between top plenum and bottom plenum test points at all plenum locations for both system excitation modes. It can only be noted that the bottom plenum data always showed a slightly higher maximum amplitude ratio. It is not known as yet how far this assumption is valid in terms of plenum volume.

2) The flexible plenum theory showed excellent agreement with test data at the plenum location for all three rpm values and for both system-excitation methods (plenum exit area modulation and duct damper area modulation) up to ~25 Hz. For the first mode, the main resonant frequency is 6 Hz, which corresponds to the flexible-plenum/duct interaction frequency, while for the second mode, the antiresonant frequency is 14 Hz, which corresponds to the duct frequency if one termination is at constant pressure and the other is at

constant flow. The success of the theory at the plenum location is quite gratifying since it is the plenum pressure that provides the lift for the surface-effect ship.

3) At the blower location, the agreement between theory and experiment is only fair. For the first excitation mode (plenum exit area modulation), there is a weak resonance at the 6-Hz plenum/duct frequency, followed by a lesser rise at the 30-Hz constant-pressure termination duct frequency. No dramatic amplitude changes occur to induce the blower to stall and surge. On the other hand, the theory predicts a sharp spike at the 30-Hz duct frequency of such a high amplitude to surely induce the blower to stall. This discrepancy must be investigated since blower stall must be avoided. For a second excitation (duct damper area modulation), there are large-amplitude experimental spikes at 19 to 22 Hz, although the theory predicts such resonances at 30 Hz, which corresponds to the constant-pressure termination duct frequency. It may be observed that the experimental resonance of ~ 20 Hz is halfway between the 28-Hz duct frequency with constant-pressure terminations and the 14-Hz duct frequency with one termination at constant pressure and the other at constant volume. In these cases, with an amplitude ratio over 5, there is a serious risk of blower stall, depending on the magnitude of the excitation and the operating point of the blower. Clearly it is most important to consider the frequency response at the blower discharge location.

4) There are six distinct experimental frequency-response patterns for the three locations and the two system-excitation modes. The agreement between theory and experiment can be considered quite satisfactory for all except the case of the blower location with first excitation mode. Further investigations therefore should be focused on that case, because of its potential impact on blower stall.

References

[1] Shih, H. H., Kaminsky, B., and Teyssandier, R. G., "Procedures and Criterion for Analyzing the Dynamic Stability of Surface Effect Ships," U.S. Navy NAVSEC Rep. 6135-75-10, Oct. 3, 1975, (Westinghouse Electric Corp., Oceanic Engineering Rep. 75-35, Oct. 3, 1975).

[2] Cummings, D., Shursky, S., Kern, E., and Yeung, R., "Mathematical Model of an Air Cushion Vehicle," U. S. Navy NTEC Rep. NAVTRAEQUIPCEN 730C-0138-1, May 1975.

[3] Schneider, J. and Kaplan, P., "The Incorporation of Fan Dynamics into the Motion Simulation of Surface Effect Ships," *Proceedings of the Fourth Ship Control Systems Symposium,* Vol. 4, Oct. 1975, pp. 4-91 to 4-116.

[4] Grant, U.S., Jr., "Study of Heave Acceleration/Velocity Control for the Surface Effect Ship," MS thesis, Naval Postgraduate School, Monterey, Calif., Dec. 1974.

[5] Myers, K. R., "Turning Characteristics of the Bell 100-Ton Surface Effect Ship," MS thesis, Naval Postgraduate School, Monterey, Calif., June 1973.

[6] Cagle, L.F., "Some Performance Characteristics of the Bell 100-Ton Surface Effect Ship," MS thesis, Naval Postgraduate School, Monterey, Calif., June 1973.

[7] Forbes, G. T., "Validation of the Nonlinear Six Degrees of Freedom Mathematical Model of the Model of the XR-3 Captured Air Bubble Surface Effect Ship in Calm Water," MS thesis, Naval Postgraduate School, Monterey, Calif., Dec. 1974.

[8] Finley, R.A., "Refinements of the Seal Subroutines and Fan Air Flow Maps for the XR-3 Loads and Motion Program," MS thesis, Naval Postgraduate School, Monterey, Calif., Dec. 1974.

[9] Rajan, J.R.N. and Csaky, T.G., "Heaving and Pitching Motion Analysis and Fan System Design for Captured Air Bubble Crafts," ASME Paper 69-WA/Au-6, Los Angeles, Calif., Nov. 1969.

[10] Goldschmied, F.R., "On the Frequency Response of Viscous Compressible Fluids as a Function of the Stokes Number," *ASME Journal of Basic Engineering,* June 1970, pp. 333-347.

[11] Cheshire, L.J., "The Design and Development of Centrifugal Compressors for Aircraft Gas Turbines," *Proceedings Institute of Mechanical Engineering,* London, Vol. 153, 1945, p. 426.

[12] Dussourd, J.L. and Putnam, W.E., "Instability and Surge in Dual-Entry Centrifugal Compressors," *Proceedings of the ASME Symposium on Compressor Stall, Surge and System Response,* 1960, p. 6.

[13] Lennemann, E. and Howard, J.H.G., "Unsteady Flow Phenomena in Rotating Centrifugal Impeller Passages," ASME Paper 69-GT-35, March 1969.

[14] Gilkey, C.H., Rogers, J.D., Wyrough, D.J., Pettersson, C.H., and Howitt, I., "Centrifugal Fan/Duct Systems Vibrations," ASME Paper 74-WA/DE-30, Nov. 1974.

[15] Durkin, J.M. and Langhi, W.E., "An investigation of the Performance of a Centrifugal Lift Fan Operating Against Sinusoidally Varying Back Pressure," 8th Canadian Symposium on Air Cushion Technology, Toronto, Canada, Sept. 1974.

[16] Sweet, L.M., Richardson, H.H., and Wormley, D.N., "Plenum Air-Cushion/Compressor-Duct Dynamic Interactions," ASME Paper 75-WA/Aut-23, Dec. 1975.

[17] Ohashi, H., "Experimental Study of the Dynamic Characteristics of Turbopumps," NASA TMX-53659, Sept. 1967.